

Differences between discontinuous and continuous soft-core attractive potentials: the appearance of density anomaly

Giancarlo Franzese

*Departament de Física Fonamental,
Facultat de Física, Universitat de Barcelona,
Diagonal 647, 08028, Barcelona, Spain.**

Abstract

Soft-core attractive potentials can give rise to a phase diagram with three fluid phases at different densities (gas, low-density liquid and high-density liquid), separated by first order phase transition lines ending in critical points. Experiments show a phase diagram with these features for phosphorous and triphenyl-phosphite. Liquid-liquid phase transition could be relevant for water, silica, liquid metals, colloids and protein solutions, among others. Here we compare two potentials with short-range soft-core repulsion and narrow attraction. One of them is a squared potential that is known to have liquid-liquid phase transition, ending in a critical point, and no anomaly in density. The normal, monotonic, behavior of density for isobaric cooling is surprising if compared with molecular liquids, such as water, where a hypothetical critical point is proposed as rationale for the anomalous behavior of density. The second potential is a continuous version of the first. We show that the phase diagram associated to this new potential has, not only the liquid-liquid phase transition, but also the density anomaly. Our result, therefore, shows that the behavior in density is strongly dependent on the derivative of the potential.

Keywords: Liquid-liquid phase transition. Density anomaly. Isotropic potential.

*Electronic address: gfranzese@ub.edu

I. INTRODUCTION

Increasing experimental, theoretical and numerical evidences are showing that single-component systems can have more than the two commonly known fluid phases: gas and liquid. There is no thermodynamic inconsistency, indeed, in hypnotizing the possible existence of a phase transition between two (or more) liquids at different densities. Direct experimental evidences of this phenomenon have been observed in liquid phosphorous [1, 2] and triphenyl phosphite [3], while consistent data exists for water [4, 5, 6, 7, 8], silica [9, 10], aluminate liquids [11], selenium [12], and cobalt [13], among others [14]. Simulations predict a liquid-liquid critical point for supercooled water [15, 16, 17, 18, 19, 20, 21], phosphorous [22], supercooled silica [9, 23, 24], and hydrogen [25]. For other substances, such as carbon, literature is contradictory [26, 27, 28].

In the last years, several models have been proposed to understand the origin of the liquid-liquid phase transition. Within this context a large interest has been focused on isotropic core-softened models [29]. The reason is twofold. On the one hand, within acceptable limitations, they are models for a variety of systems including liquid metals, metallic mixtures, electrolytes, colloids and protein solution, as well as anomalous liquids, like water and silica [30, 31, 32, 33, 34, 35, 36, 37, 38, 39, 40, 41]. On the other hand, their simple definition encourages to investigate the possibility of an intriguing relation between the liquid-liquid phase transition and the anomalies in specific observables, such as the density or the diffusivity, in network-forming liquids, like water and silica.

Different kinds of isotropic potentials with soft-core have been proposed. In many of them, with the soft-core given by a Gaussian core [42] or a ramp, the presence of a liquid-liquid phase transition is observed together with anomalies in the density, in the diffusion and in the structure [39, 40, 43, 44, 45, 46, 47, 48]. This is consistent with what is proposed for water on the basis of simulations and theoretical calculations for specific models [15, 18, 21, 29].

In other attractive isotropic potentials, with the soft-core given by a square shoulder, the liquid-liquid phase transition occurs in absence of density anomaly [49, 50, 51, 52]. Nevertheless, an asymptotic tendency to the density anomaly is observed in three dimensions [50], and thermodynamic and dynamic anomalies has been found in related models in two dimensions on lattices [53] or off-lattice [45, 54].

Here we focus on the study of a potential that is the smooth version of the one with

square shoulder and attractive well which we studied in Ref. [49]. We find that the new continuous potential has a liquid-liquid phase transition, as well as the previous squared potential, consistent with the minimal difference between the two models. Nevertheless, the difference is enough to cause the appearance of the density anomaly. Hence, the anomalous behavior is strongly dependent on the fine details of the potential, including its derivative.

II. THE CONTINUOUS POTENTIAL

We consider the following isotropic pairwise potential

$$U_0(r) = \frac{U_R}{1 + \exp[\Delta(r - R_R)/a]} - U_A \exp\left[-\frac{(r - R_A)^2}{2\delta_A^2}\right] + \left(\frac{a}{r}\right)^{24}, \quad (1)$$

where U_R and U_A are the energy of the repulsive shoulder and of the attractive well, respectively; a , R_R and R_A are the hard-core distance, the repulsive average radius and the distance of the attractive minimum, respectively; Δ is a parameter related to the slope of the potential at R_R ; δ_A^2 is the variance of the Gaussian centered at R_A .

For the set of parameters $U_R/U_A = 2$, $R_R/a = 1.6$, $R_A/a = 2$, $\Delta = 15$, $(\delta_A/a)^2 = 0.1$, at distance $r/a = 3$ the value of the potential is $U_0/U_A \simeq -6.7 \times 10^{-3}$, with $U_0 \rightarrow 0$ for $r/a > 3$. Hence, to reduce the computational effort, we set a potential cutoff at $r/a = 3$ and add a constant and a linear term to the potential in order to have both the potential and its r -derivative equal to zero at the cutoff.

The resulting potential is

$$U(r) = U_0(r) + CU_A + B\frac{r}{a} \quad (2)$$

where, for our choice of parameters and cutoff distance $r_c/a = 3$, the dimensionless constants are set to $C = 0.208876$ and $B = -0.0673794$. The approximate attractive width, calculated as the width at half height of the Gaussian function defining the attractive well, is $w_A = 2\delta_A\sqrt{2\ln(2)} \simeq 0.75 a$.

The continuous potential smoothly follows the corresponding squared one (Figure 1). While the continuous potential is defined by five parameters (plus the cutoff distance and two additional constants), the squared potential is defined by only three parameters: U_R/U_A , the repulsive width $w_R/a = (R_R - a)/a$ of the shoulder and the attractive width w_A/a of the

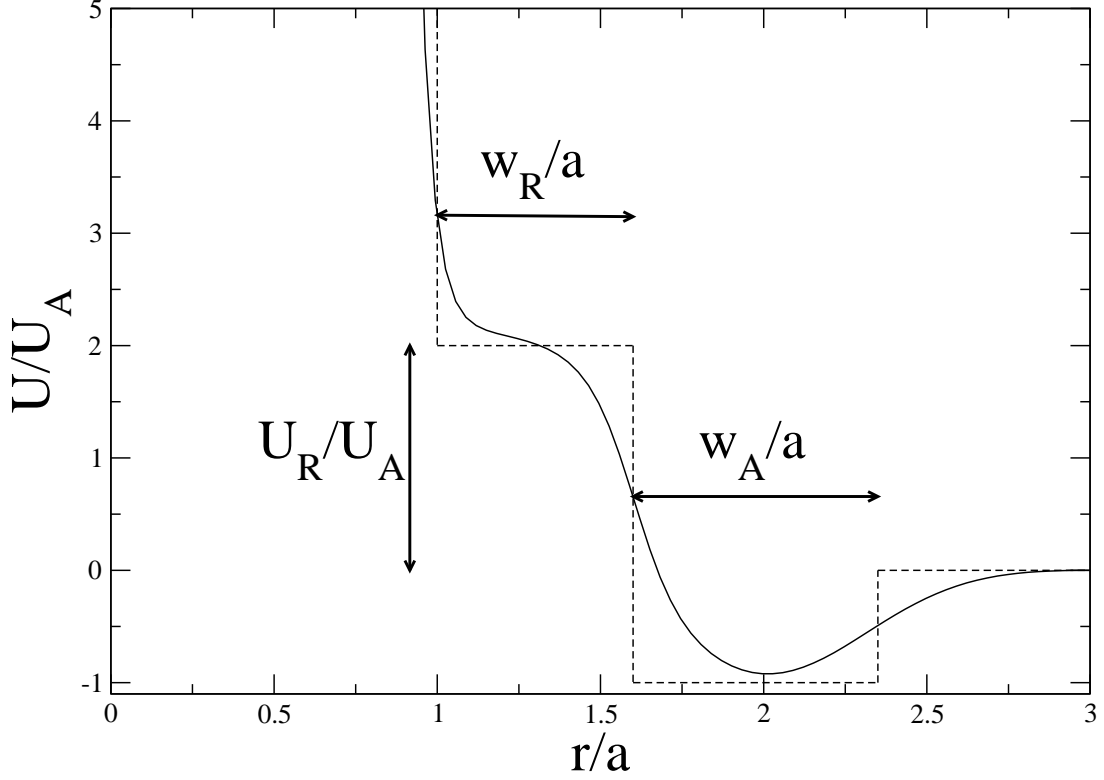


FIG. 1: Isotropic pairwise interaction potential in Eq. (1), for the parameters in the text (continuous line), compared with the squared potential (dashed line) of Refs. [49, 50, 51, 52] for $U_R/U_A = 2$, repulsive width $w_R/a = 0.6$ and attractive width $w_A/a = 0.75$. The two potentials have the same U_R/U_A , the same repulsive range $w_R = (R_R - a)$ and the same attractive width $w_A = 2\delta_A\sqrt{2\ln(2)}$. The continuous potential crosses the lines of the shoulder and well of the squared potential approximately in the middle.

well. A straightforward correspondence between the two types of potential can be established by choosing the same U_R/U_A , the same $w_R = (R_R - a)$ and $w_A = 2\delta_A\sqrt{2\ln(2)}$, respectively.

The squared potential is more appropriate for a systematic study of the phase diagram changes for different combinations of parameters. This analysis has been performed in Refs. [50, 51, 52]. The continuous potential, on the other hand, resembles effective pair potentials obtained from the second-order pseudo-potential perturbation theory for liquid alkaline-earth metals, such as magnesium, calcium, strontium and barium near the melting point [55, 56], or effective potentials for colloidal mono-layers at the water-air interface given by inversion of structural data [57].

Moreover, the angle-average of several asymmetric water potentials give rise to isotropic soft-core effective interactions, such as the one studied in Refs. [58, 59]. Hence, the continuous potential appears to be a more realistic model for different problems.

III. MOLECULAR DYNAMICS SIMULATIONS

We perform Molecular Dynamics (MD) simulations in the NVT ensemble for $N = 1372$ particles of unit mass m in a cubic box of volume V with periodic boundary conditions at temperature T . We use standard MD technique for continuous potentials, with velocity Verlet integrator [60]. We keep T constant by rescaling the velocities at each time step by a factor of $(T/\mathcal{T})^{1/2}$ where \mathcal{T} is the current kinetic temperature and T is the desired thermodynamic temperature [60]. We calculate the pressure P by means of its expression in terms of the second virial coefficient [60].

We consider 28 densities $\rho \equiv N/V$ in the range $0.05 \leq \rho a^3 \leq 0.33$ and 5 temperatures in the range $0.4 \leq k_B T/U_A \leq 1.9$, where k_B is the Boltzmann constant. For each state point we run 8 independent simulations from different configurations equilibrated at $T + \delta T$, with $k_B \delta T/U_A = 0.1$ for the state points with $0.4 \leq k_B T/U_A \leq 0.8$, and with $k_B \delta T/U_A = 0.2$ for the state points with $0.9 \leq k_B T/U_A \leq 1.9$.

Each run has 10^6 MD steps, with a time step $\delta t = 3.2 \times 10^{-3}$ times units, where time is measured in units of $(a^2 m/U_A)^{1/2}$ (of the order of $\approx 2.1 \times 10^{-12}$ s for argon-like atoms and $\approx 1.7 \times 10^{-12}$ s for water-like molecules). We record pressure and potential energy every $\Delta t = 100$ MD steps. For the calculation of the averages we consider only the data corresponding to states that are stable within the simulation time, as follows from the analysis of the time series of pressure, average temperature, and potential energy. Usually an equilibration time of 10^5 MD steps is enough to reach a stable state. We average the data binned in 10^3 consecutive MD steps, a time that we test to be enough to decorrelate the data for the considered state points.

For densities $0.275 \leq \rho a^3 \leq 0.330$ at $k_B T/U_A = 0.5$, and for $\rho a^3 \geq 0.21$ at $k_B T/U_A = 0.4$, we observe spontaneous crystallization during the simulation time. To get data for the metastable liquid phase in these cases, instead of annealing from an equilibrium configuration at $T + \delta T$, we perform instantaneous quenches from configurations equilibrated at $k_B T/U_A = 0.8$. Next, we analyze the evolution in time of the structure factor, as described in details in

Ref. [50], and we use for the averages only the data corresponding to the metastable liquid state. We accumulate statistics for these state points up to reach a number of independent metastable configurations comparable to the number used for the other state points. We try to analyze in the same way also data for quenches to $k_B T/U_A = 0.3$ and lower T , but the crystal nucleation time observed in these cases is too small to allow us reliable estimations.

IV. THE PHASE DIAGRAM

We analyze the isotherms in the P - ρ phase diagram. At low density (Figure. 2) we observe non-monotonic isotherms, showing a maximum at low ρ and a minimum at higher ρ (the so-called *loop*), typical of a first-order phase transition between two coexisting phases. By joining these minima and maxima we get an estimate of the two branches of the spinodal line, i. e. the limit of stability of one of the two coexisting phases with respect to the other. The point where the two branches of the spinodal line meet (the *vertex* of the spinodal) is, by definition, the gas-liquid critical point C_1 , with critical pressure P_{C_1} , density ρ_{C_1} and temperature T_{C_1} . Since, by definition, at ρ_{C_1} the ρ -derivative of the critical isotherm $P(\rho, T_{C_1})$ is zero, we interpolate our data to find the isotherm that appears to be flat around the approximate vertex of the spinodal line. Our final estimate of the parameters for the gas-liquid critical point is $\rho_{C_1} a^3 = 0.08 \pm 0.02$, $P_{C_1} a^3/U_A = 0.021 \pm 0.008$, and $k_B T_{C_1}/U_A = 0.96 \pm 0.06$.

At higher density we observe that isotherms for $k_B T/U_A \leq 0.8$ show a clear minimum in the derivative of P with respect to ρ (Figure 3) approaching zero at $k_B T/U_A = 0.5$ and $\rho a^3 \approx 0.25$. If we assume that the isotherms below this temperature behave in a regular way and with continuity with respect to the isotherms at higher T , then Figure 3 shows that the isotherm at $k_B T/U_A = 0.5$ is just above the critical isotherm, where $(\partial P/\partial \rho)_T = 0$. This is confirmed by the analysis of the state points equilibrated at $k_B T/U_A = 0.4$ (small open circles in Figure 4) showing a clear maximum in pressure at $\rho a^3 \approx 0.21$, as expected for an isotherm entering into the instability region delimited by a spinodal line. Direct observation of the *loop* along the isotherm at $k_B T/U_A = 0.4$ is hindered by the fast nucleation of the crystal, as described in the previous section.

To estimate the parameters of this high-density critical point C_2 , we extrapolate from the available isotherms at higher T , the high- ρ state points for $k_B T/U_A = 0.4$. The re-

sulting curve [the lowest continuous line in Figure 4(a) and Figure 4(b)] is in very good agreement with the state points calculated at $0.20 \leq \rho a^3 \leq 0.22$, confirming the validity of the assumption of continuity and regularity with respect to the isotherms at higher T .

Therefore, our simulation show a critical point C_2 between two liquids at high ρ and below the gas–liquid critical temperature, as seen for the squared soft-core shouldered potential studied in Refs. [49, 50, 51, 52] (Figure 1). The high density liquid is metastable with respect to the spontaneous crystallization and the crystal nucleation process is very fast around C_2 . The interpolation of the data allows us to estimate the critical parameters of the liquid-liquid critical point C_2 as $\rho_{C_2} a^3 = 0.248 \pm 0.007$, $P_{C_2} a^3 / U_A = 0.286 \pm 0.006$, and $k_B T_{C_2} / U_A = 0.49 \pm 0.01$.

V. COMPARISON WITH THE PHASE DIAGRAM OF THE SQUARED POTENTIAL

We compare the phase diagram found here with the phase diagram for the corresponding squared potential (Figure 1) with parameters $U_R/U_A = 2$, $w_R/a = 0.6$ and $w_A/a = 0.75$. The phase diagram of the squared potential with the straightforward correspondence to the one studied here is not available in literature, however, in Ref. [51] we studied a squared potential with set of parameters $U_R/U_A = 2$, $w_R/a = 0.6$ and $w_A/a = 0.7$ (see Figure 3 of Ref. [51]). Comparison with this potential is shown in Table I.

TABLE I: Temperatures T_{C_1} and T_{C_2} , pressures P_{C_1} and P_{C_2} , and densities ρ_{C_1} and ρ_{C_2} , for the critical points C_1 and C_2 , respectively, computed for the continuous potential presented in this work and the squared potential with parameters $U_R/U_A = 2$, $w_R/a = 0.6$ and $w_A/a = 0.7$ in Ref. [51].

Potential	$k_B T_{C_1} / U_A$	$a^3 P_{C_1} / U_A$	$a^3 \rho_{C_1}$	$k_B T_{C_2} / U_A$	$a^3 P_{C_2} / U_A$	$a^3 \rho_{C_2}$
Continuous	0.96 ± 0.06	0.021 ± 0.008	0.08 ± 0.02	0.49 ± 0.01	0.286 ± 0.006	0.248 ± 0.007
Squared	1.24 ± 0.01	0.03 ± 0.01	0.09 ± 0.02	0.69 ± 0.02	0.11 ± 0.02	0.28 ± 0.02

The comparison shows that the critical parameters of the gas–liquid critical point C_1 are almost the same in the two cases with lower values for the continuous potential. The percentage of variation is 11% for ρ_{C_1} , 23% T_{C_1} , and 30% for P_{C_1} .

For the liquid–liquid critical point C_2 the parameter ρ_{C_2} of the continuous potential decreases of the same percentage 11% of the critical density of C_1 , and T_{C_2} decreases of 29%, a percentage comparable to the decrease of T_{C_1} . The situation is different, instead, for the variation of P_{C_2} , that increases of 61% in the continuous case with respect to the case of the squared potential.

Therefore, the largest difference between the squared and the continuous case is on the pressure of the critical points, with a considerable increase of P_{C_2} . These effects are consistent with the analysis performed in Refs. [51, 52] for a decrease of the attractiveness of a squared potential, as a consequence of the decrease of the range of the attractive well w_A , or the increase of the repulsive energy U_R/U_A . Panels (a), (b), (c), (g), (h), (i) of Figure 9 of Ref. [51], indeed, show that a decrease of w_A , or an increase of U_R/U_A , determines the increase of P_{C_2} and the decrease of T_{C_2} , while the other critical parameters for C_1 and C_2 are almost unaffected.

Hence, the continuous potential studied here behaves like a squared potential less attractive than the one that would be in straightforward correspondence with it. This is consistent, with the observation that the volume integral of the attractive part of the present potential is smaller than the volume integral for the corresponding squared potential, while the volume integral for the repulsive part is approximately the same in both potentials.

As predicted in Ref. [52], this continuous potential with two critical points satisfy the empirical relation

$$-2 \lesssim \frac{1}{U_A V_{SC}} \int_a^\infty U(r) d\vec{r} \lesssim 1, \quad (3)$$

where $V_{SC} \equiv \frac{2\pi}{3} R_R^3$. With the present choice of parameters we find that the integral in Eq.(3) has a numerical value of ≈ -0.88 , supporting the idea that the Eq.(3) is a good empirical relation to predict if an isotropic potential could display a phase diagram with two critical points.

VI. DENSITY ANOMALY

A closer look at the high-density part of the P – ρ phase diagram [Figure 4(b)] shows that at low T , close to C_2 , the isotherms cross at various densities. This is a clear signal of a density anomaly.

Indeed, the crossing of isochores implies $(\partial P/\partial T)_V = 0$, i.e., for one of the Maxwell rela-

tions, $(\partial S/\partial V)_T = 0$, where S is the entropy. Hence, is $(\partial S/\partial P)_T = (\partial S/\partial V)_T (\partial V/\partial P)_T = 0$, where we use the fact that $(\partial V/\partial P)_T < 0$ is finite for liquids. Hence, for one of the Maxwell relations, is $(\partial V/\partial T)_P = 0$, or equivalently $(\partial \rho/\partial T)_P = 0$. Since at high enough T the isobaric density increases on decreasing T , this relation implies that there is a temperature of maximum density T_{MD} at constant P (Figure 5).

For $T > T_{\text{MD}}$ the isobaric density decreases for increasing T , as for normal liquids, while for $T < T_{\text{MD}}$ it decreases for decreasing T , giving rise to an anomalous behavior in density. This can be seen in a clear way by studying directly the $(\partial P/\partial T)_\rho$ (Figure 6). Comparison with Figure 4(b) shows that the isochores with a minimum, i.e. $(\partial P/\partial T)_\rho = 0$, correspond to the densities where the isotherms cross in the P - ρ phase diagram.

VII. DISCUSSION AND CONCLUSIONS

Our results show that the continuous interaction potential presented here has a maximum in density along the T_{MD} line. This anomaly in density is typical of network-forming liquids, such as water or SiO_2 [19, 29, 61], and has been observed in other soft-core potentials [39, 40, 41, 43, 44, 45, 46, 47, 48]. In the present model, as well as in those for water and other anomalous liquids [29] the T_{MD} line converges toward a liquid-liquid critical point, i.e. C_2 in this work. This observation has been often considered as an evidence for the fact that the liquid-liquid critical point implies the presence of a T_{MD} line.

On the other hand, we know that for the squared soft-core potential the liquid-liquid critical point occurs in absence of the density anomaly, as shown by the extensive analysis performed in Ref. [50]. As it was observed (see Figure 21 in Ref. [50]), the squared potential does not satisfy the condition for the density anomaly, Eq.(21) in Ref. [50], but approaches that condition in an asymptotic way. Hence, is not clear if the absence of the T_{MD} is a consequence of the specific discontinuous shape of the squared potential.

Since the continuous potential presented here can be tuned to approximate in a close way the discontinuity at R_R for the squared potential (Figure 7), it could be interesting to study the effect on T_{MD} of the variation of the parameters Δ (determining the slope at the R_R) of the continuous potential. Such a study could shed light on the relevant question about the relation between the liquid-liquid critical point and the presence of the density anomaly. It is worth to observe here that the implication of the presence of a liquid-liquid critical

point for network-forming molecular liquids with anomalous density has been supported by extensive studies on water-like models (see for example Refs. [16, 17, 18]).

In conclusion, we have presented here a continuous soft-core potential with a shape which resembles that of effective interaction potentials for liquid metals [55] or colloid solutions [57]. The model displays a phase diagram with a high- T gas-liquid critical point C_1 at low density, and a low- T liquid-liquid critical point C_2 at high density, occurring at the limit of stability, within the simulation time, of the liquid phase with respect to the crystal.

Comparison with the case of the soft-core squared potentials [49, 50, 51, 52] shows that the continuous potential is less attractive than its straightforward corresponding squared potential. The main qualitative difference with the case of squared potentials is that the continuous potential shows the density anomaly, typical of network-forming liquids such as water, and observed in other soft-core potentials [39, 40, 41, 43, 44, 45, 46, 47, 48]. Further investigation is necessary to understand how the appearance of this anomaly is related to the parameters of the potential.

Acknowledgments

We thank S. Mossa and F. W. de Sousa Lima that helped in different stages of this work. We acknowledge the allocation of computer resources from INFM Progetto Calcolo Parallelo at CINECA, Italy. We thank the Spanish Ministerio de Educación y Ciencia for financial support within the Programa Ramón y Cajal and Grant No. FIS2004-03454.

-
- [1] Y. Katayama, T. Mizutani, W. Utsumi, O. Shimomura, M. Ya-makata, and K. Funakoshi, *Nature* **403**, (2000) 170; Y. Katayama, Y. Inamura, T. Mizutani, M. Yamakata, W. Utsumi, and O. Shimomura, *Science* **306**, (2004) 848.
 - [2] G. Monaco, S. Falconi, W. A. Crichton, and M. Mezouar, *Phys. Rev. Lett.* **90**, (2003) 255701.
 - [3] H. Tanaka, R. Kurita, and H. Mataka, *Phys. Rev. Lett.* **92**, (2004) 025701; R. Kurita and H. Tanaka, *Science* **306**, (2004) 845.
 - [4] O. Mishima and H. E. Stanley, *Nature* **396**, (1998) 329; O. Mishima, *Phys. Rev. Lett.* **85**, (2000) 334.
 - [5] M. C. Bellissent-Funel, *Nuovo Cimento* **20D**, 2107 (1998).

- [6] A. K. Soper and M. A. Ricci, Phys. Rev. Lett. **84**, 2881 (2000).
- [7] Y. Suzuki and O. Mishima, Nature **491**, 599 (2002).
- [8] T. Loerting, C. Salzmann, I. Kohl, E. Mayer, and A. Hallbrucker, Phys. Chem. Chem. Phys. **3**, 5355 (2001).
- [9] C. A. Angell, S. Borick, and M. Grabow, J. Non-Cryst. Solids **207**, 463 (1996); P. H. Poole, M. Hemmati, and C. A. Angell, Phys. Rev. Lett. **79**, 2281 (1997).
- [10] D. J. Lacks, Phys. Rev. Lett. **84**, 4629 (2000).
- [11] S. Aasland and P. F. McMillan, Nature **369**, 633 (1994); M. C. Wilding and P. F. McMillan, J. Non-Cryst. Solids **293**, 357 (2001).
- [12] V. V. Brazhkin, E. L. Gromnitskaya, O. V. Stalgorova, and A. G. Lyapin, Rev. High Pressure Sci. Technol. **7**, 1129 (1998).
- [13] M. G. Vasin and V. I. Ladýanov, Phys. Rev. E **68**, 051202 (2003).
- [14] P. F. McMillan, J. Mat. Chem. **14**, 1506 (2004).
- [15] P. H. Poole, F. Sciortino, U. Essmann, and H. E. Stanley, Nature **360**, 324 (1992).
- [16] G. Franzese and H. E. Stanley, J. Phys.-Cond. Mat. **14**, 2201 (2002).
- [17] G. Franzese and H. E. Stanley, Physica A, **314**, 508 (2002).
- [18] G. Franzese, M. I. Marques, and H. E. Stanley, Phys. Rev. E **67**, 011103 (2003).
- [19] G. Franzese and H. E. Stanley, J. Phys.: Cond. Mat., in print (2007).
- [20] F. Sciortino, E. La Nave, and P. Tartaglia, Phys. Rev. Lett. **91**, 155701 (2003).
- [21] I. Brovchenko, A. Geiger, and A. Oleinikova, J. Chem. Phys. **123**, 044515 (2005).
- [22] T. Morishita, Phys. Rev. Lett. **87**, 105701 (2001).
- [23] I. Saika-Voivod, F. Sciortino and P. H. Poole, Phys. Rev. E **63**, 011202-1 (2001).
- [24] S. Sastry and C. A. Angell, Nature Mater. **2**, 739 (2003).
- [25] S. Scandolo, Proc. Nat. Acad. Sci. USA **100** 3051 (2003).
- [26] M. van Thiel and F. H. Ree, Phys. Rev. B **48**, 3591 (1993).
- [27] J. N. Glosli and F. H. Ree, Phys. Rev. Lett. **82**, 4659 (1999).
- [28] L. M. Ghiringhelli, J. H. Los, E. J. Meijer, A. Fasolino, and D. Frenkel, Phys. Rev. Lett. **94**, 145701 (2005).
- [29] P. Debenedetti, J. Phys.: Cond. Mat. **15**, R1669 (2003).
- [30] P. C. Hemmer and G. Stell, Phys. Rev. Lett. **24**, 1284 (1970); G. Stell and P. C. Hemmer, J. Chem. Phys. **56**, 4274 (1972).

- [31] P. G. Debenedetti, *Metastable Liquids: Concepts and Principles* (Princeton University Press, Princeton, 1998); *Hydration Processes in Biology. Theoretical and Experimental Approaches*, Vol. 305 of NATO Advanced Studies Institute, Series A: Life Sciences, edited by M. C. Bellissent-Funel (IOS Press, Amsterdam, 1998).
- [32] M. Silbert and W. H. Young, Phys. Lett. **58A**, 469 (1976); D. Levesque and J. J. Weis, *ibid.* **60A**, 473 (1977); J. M. Kincaid and G. Stell, *ibid.* **65A**, 131 (1978).
- [33] W. M. Shyu, J. H. Wehling, and M. R. Cordes, Phys. Rev. B **4**, 1802 (1971); M. Appapillai and V. Heine, Cavendish Laboratory Technical Report No. 5, 1972 (unpublished); K. K. Mon, N. W. Ashcroft, and G. V. Chester, Phys. Rev. B **19**, 5103 (1979).
- [34] J. M. Lawrence, M. C. Croft, and R. D. Parks, Phys. Rev. Lett. **35**, 289 (1975).
- [35] P. G. Debenedetti, V. S. Raghavan, and S. S. Borick, J. Phys. Chem. **95**, 4540 (1991).
- [36] F. H. Stillinger and T. Head-Gordon, Phys. Rev. E **47**, 2484 (1993).
- [37] S. S. Borick, P. G. Debenedetti, and S. Sastry, J. Phys. Chem. **99**, 3781 (1995); T. M. Truskett, P. G. Debenedetti, S. Sastry, and S. Torquato, J. Chem. Phys. **111**, 2647 (1999).
- [38] M. R. Sadr-Lahijany, A. Scala, S. V. Buldyrev, and H. E. Stanley, Phys. Rev. Lett. **81**, 4895 (1998); Phys. Rev. E **60**, 6714 (1999); A. Scala, M. R. Sadr-Lahijany, N. Giovambattista, S. V. Buldyrev, H. E. Stanley, *ibid.* **63**, 041202 (2001); J. Stat. Phys. **100**, 97 (2000).
- [39] E. A. Jagla, Phys. Rev. E **58**, 1478 (1998); J. Chem. Phys. **110**, 451 (1999); J. Chem. Phys. **111**, 8980 (1999); Phys. Rev. E **63**, 061501 (2001); Phys. Rev. E **63**, 061509 (2001).
- [40] N. B. Wilding and J. E. Magee, Phys. Rev. E **66**, 031509 (2002); H. M. Gibson, N. B. Wilding, Phys. Rev. E **74**, 019903 (2006).
- [41] J. B. Caballero, A. M. Puertas, Phys. Rev. E **74**, 051506 (2006).
- [42] F. H. Stillinger and T. A. Weber, J. Chem. Phys. **68**, 3837 (1978).
- [43] P. Kumar, S. V. Buldyrev, F. Sciortino, E. Zaccarelli, and H. E. Stanley, Phys. Rev. E **72**, 021501 (2005); Z. Yan, S. V. Buldyrev, N. Giovambattista, and H. E. Stanley, Phys. Rev. Lett. **95**, 130604 (2005); L. Xu, P. Kumar, S. V. Buldyrev, S.-H. Chen, P. Poole, F. Sciortino, and H. E. Stanley, Proc. Natl. Acad. Sci. U.S.A. **102**, 16558 (2005); L. Xu, S. Buldyrev, C. A. Angell, and H. E. Stanley, Phys. Rev. E **74**, 031108 (2006); Z. Yan, S. V. Buldyrev, N. Giovambattista, P. G. Debenedetti, and H. E. Stanley, Phys. Rev. E **73**, 051204 (2006).
- [44] R. Sharma, A. Mudi, and C. Chakravarty, J. Chem. Phys. **125**, 044705 (2006). R. Sharma, S. N. Chakraborty, and C. Chakravarty, J. Chem. Phys. **125**, 204501 (2006).

- [45] P. Camp, Phys. Rev. E **68**, 061506 (2003); Phys. Rev. E **71**, 031507 (2005).
- [46] R. Esposito, F. Saija, A. M. Saitta, P. V. Giaquinta, Phys. Rev. E **73**, 040502 (2006).
- [47] A. B. de Oliveira, P. A. Netz, T. Colla, and M. C. Barbosa, J. Chem. Phys. **124**, 084505 (2006); J. Chem. Phys. **125**, 124503 (2006).
- [48] J. Mittal, J. R. Errington, and T. M. Truskett, J. Chem. Phys. **125**, 076102 (2006).
- [49] G. Franzese, G. Malescio, A. Skibinsky, S.V. Bulderyev, and H. E. Stanley, Nature **409**, 692 (2001).
- [50] G. Franzese, G. Malescio, A. Skibinsky, S. V. Buldyrev, and H. E. Stanley, Phys. Rev. E **66**, 051206 (2002).
- [51] A. Skibinsky, S.V. Buldyrev, G. Franzese, G. Malescio, and H. E. Stanley, Phys. Rev. E **69**, 061206 (2004).
- [52] G. Malescio, G. Franzese, A. Skibinsky, S. V. Buldyrev, and H. E. Stanley, Phys. Rev. E **71**, 061504 (2005).
- [53] A. L. Balladares and M. C. Barbosa, J. Phys.: Cond. Matter **16**, 8811 (2004). A. B. de Oliveira and M. C. Barbosa, J. Phys.: Cond. Matter **17**, 399 (2005). V. B. Henriques and M. C. Barbosa, Phys. Rev. E **71**, 031504 (2005). V. B. Henriques, N. Guissoni, M. A. Barbosa, M. Thielo, and M. C. Barbosa, Mol. Phys. **103**, 3001 (2005).
- [54] A. Scala, M. R. Sadr-Lahijany, N. Giovambattista, S. V. Buldyrev, and H. E. Stanley, J. Stat. Phys. **100**, 97 (2000); Phys. Rev. E **63**, 041202 (2001). S. V. Buldyrev, G. Franzese, N. Giovambattista, G. Malescio, M. R. Sadr-Lahijany, A. Scala, A. Skibinsky, and H. E. Stanley, Physica A **304**, 23 (2002). S. V. Buldyrev and H. E. Stanley, Physica A **330**, 124 (2003).
- [55] See for example, F. Wax, R. Albaki, and J.-L. Bretonnet, Phys. Rev. B **62**, 14818 (2000).
- [56] P. G. Debenedetti, V. S. Raghavan, and S.S. Borick, J. Phys. Chem. **95**, 4540 (1991) and references therein.
- [57] M. Quesada-Pérez, A. Moncho-Jordá, F. Martínez-López, and R. Hidalgo-Álvarez J. Chem. Phys. **115**, 10897 (2001).
- [58] C. H. Cho, Surjit Singh, and G. W. Robinson Phys. Rev. Lett. **76**, 1651 (1996).
- [59] P. A. Netz, J. F. Raymundi, A. S. Camera, and M. C. Barbosa, Physica A **342**, 48 (2004).
- [60] M.P. Allen and D.J. Tildesley, *Computer Simulation of Liquids*, Oxford University Press, New York, 1989.
- [61] P. G. Debenedetti and H. E. Stanley, Physics Today **56** 40 (2003).

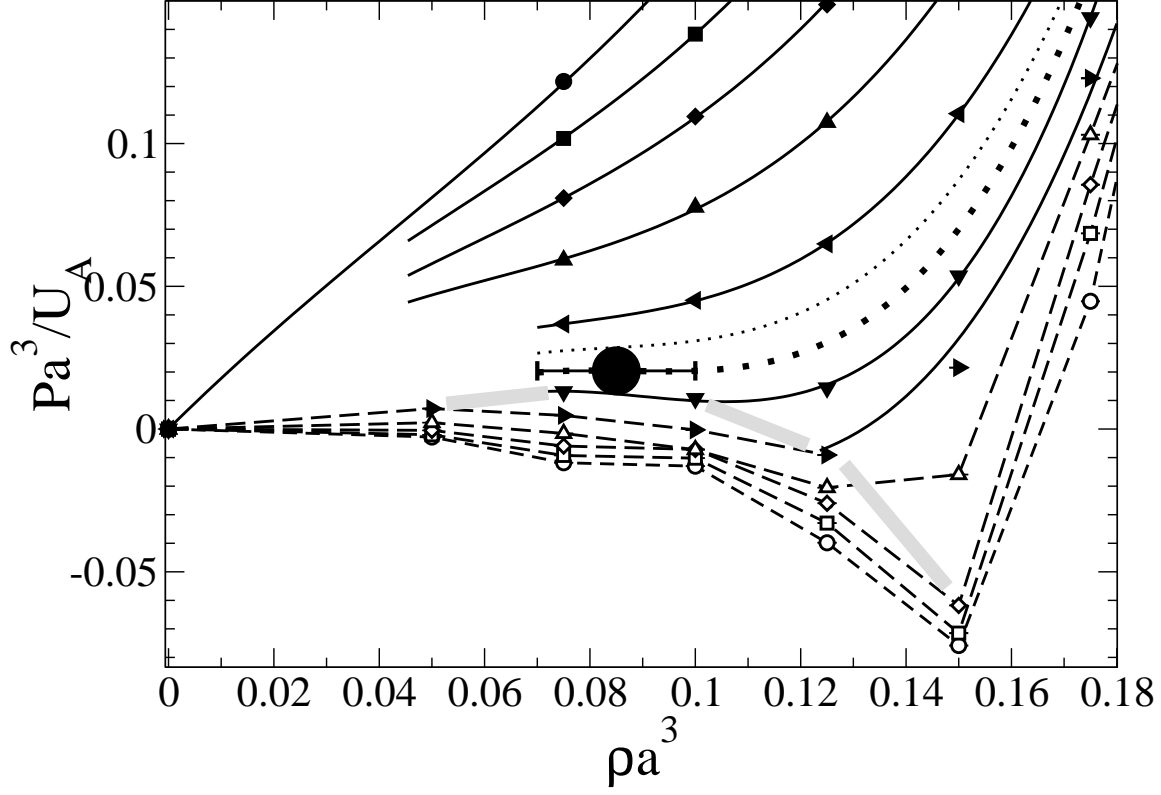


FIG. 2: Low density phase diagram with the estimate of the gas-liquid critical point C_1 (large full circle) at $\rho_{C_1} a^3 = 0.08 \pm 0.02$, $P_{C_1} a^3 / U_A = 0.021 \pm 0.008$, and $k_B T_{C_1} / U_A = 0.96 \pm 0.06$. Symbols are state points calculated with MD in the pressure-density (P - ρ) plane for, from top to bottom, $k_B T / U_A = 1.9, 1.7, 1.5, 1.3, 1.1, 0.9, 0.8, 0.7, 0.6, 0.5, 0.4$. Full lines are cubic interpolations of the isotherms. Dashed lines are a guide for the eyes connecting symbols for the isotherms at which the cubic interpolation is not reliable. Dotted lines are linear interpolations between the isotherm at $k_B T / U_A = 1.1$ and the isotherm at $k_B T / U_A = 0.9$ for (upper thin dotted line) $k_B T / U_A = 1.02$ and (lower thick dotted line) $k_B T / U_A = 0.96$, approximating the critical isotherm. The thick gray dashed line at $T < T_{C_1}$ is a guide for the eyes connecting the points of minimum P along the isotherms for $\rho > \rho_{C_1}$ (i. e. the limit of stability of the liquid with respect to the gas), and the points of maximum P for $\rho < \rho_{C_1}$ (i. e. the limit of stability of the gas with respect to the liquid), and representing an estimate of the spinodal line. Errors on state points are smaller than symbols size.

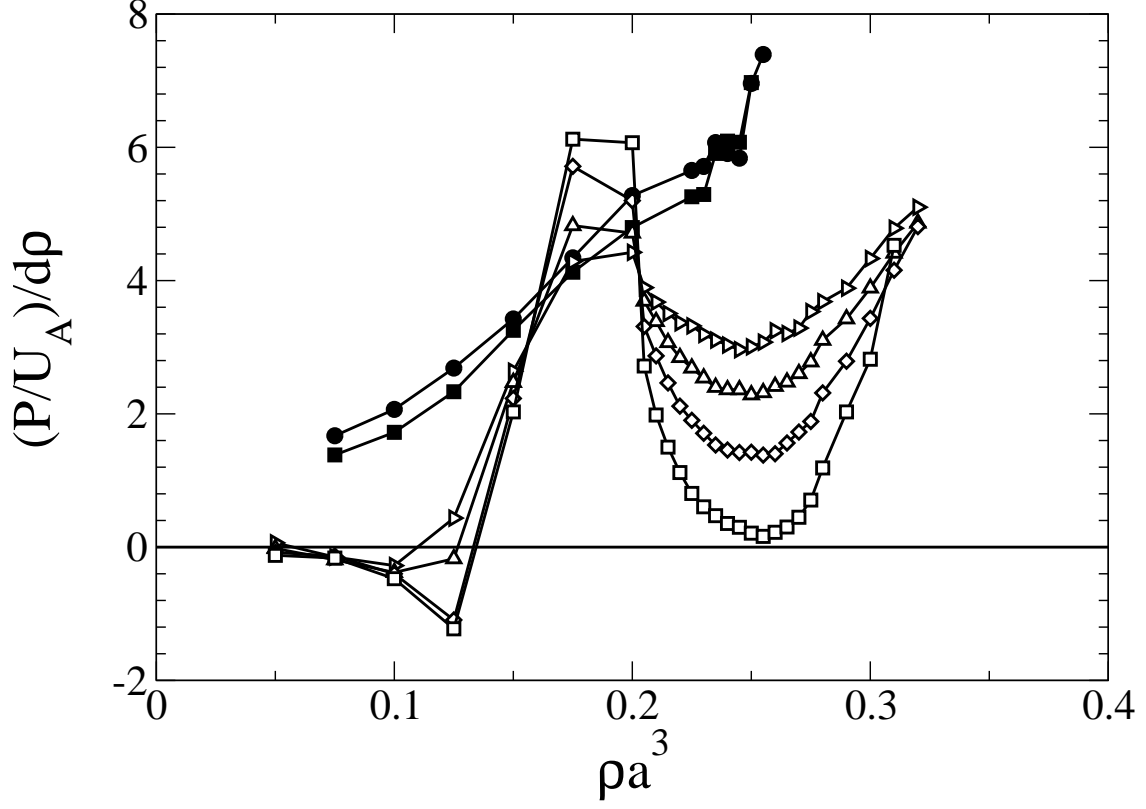


FIG. 3: Numerical derivative of P with respect to ρ along the isotherms at, from top to bottom, $k_B T/U_A = 1.9, 1.7, 0.8, 0.7, 0.6, 0.5$. Symbols are as in Figure 2. At high T the derivative increases with ρ as for normal liquids, while at low T the derivative is non monotonic with a clear minimum that approaches zero for $k_B T/U_A = 0.5$ at density $\rho a^3 \approx 0.25$. Errors on state points are smaller than symbols size.

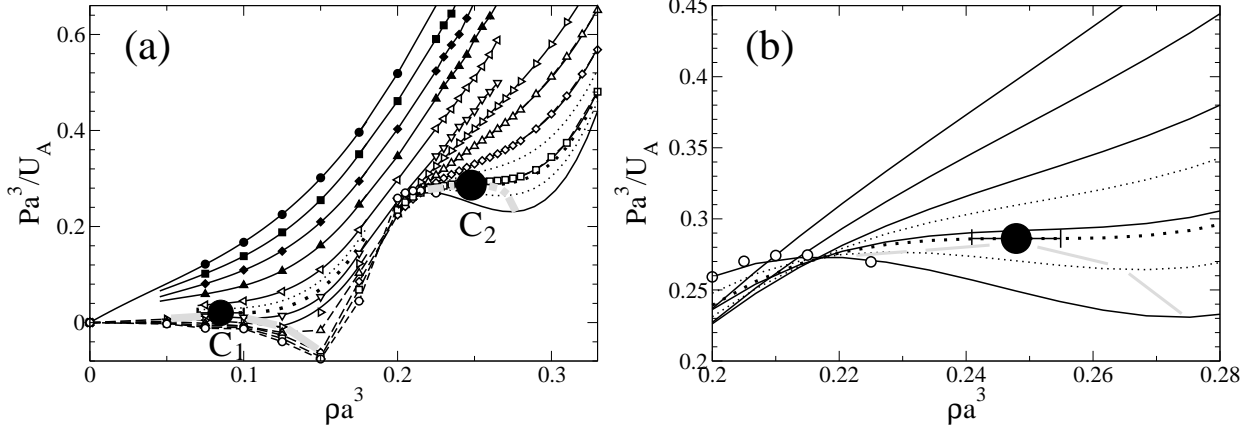


FIG. 4: (a) Complete phase diagram with the gas-liquid critical point C (large full circle) as shown in Figure 2, and the liquid-liquid critical point C_2 (large open circle) estimated at $\rho_{C_2} a^3 = 0.248 \pm 0.007$, $P_{C_2} a^3 / U_A = 0.286 \pm 0.006$, and $k_B T_{C_2} / U_A = 0.49 \pm 0.01$. Symbols and lines are as in Figure 2. The lowest solid line below C_2 is an extrapolation of the data at $k_B T / U_A = 0.4$ in the region of inevitable crystallization, on the basis of the interpolation of the isotherms at higher temperatures. This extrapolation shows very good agreement with the state points that can be directly calculated at $k_B T / U_A = 0.4$ (small open circles). In the high- ρ region, from top to bottom, the upper thin dotted line is the interpolation at $k_B T / U_A = 0.55$ between consecutive isotherms, the thick dotted line is the interpolated critical isotherm, and the lowest thin dotted line is the interpolations for $k_B T / U_A = 0.45$. The thick gray dashed line at $T < T_{C_2}$ is a guide for the eyes connecting the points of minima and maxima of P along the isotherms representing an estimate of the liquid-liquid spinodal line. (b) The high- ρ portion of the phase diagram, around the liquid-liquid critical point C_2 . Symbols and lines are as in the previous panel. For sake of clarity we show only the lines corresponding at the interpolations of the data along the isotherms for $0.4 \leq k_B T / U_A \leq 0.8$. The agreement between the data at $k_B T / U_A = 0.4$ (open circles) and the extrapolation of the corresponding isotherm (lowest solid line) on the basis of the data at higher T is remarkable. In both panels, when not shown, errors are smaller than symbols size.

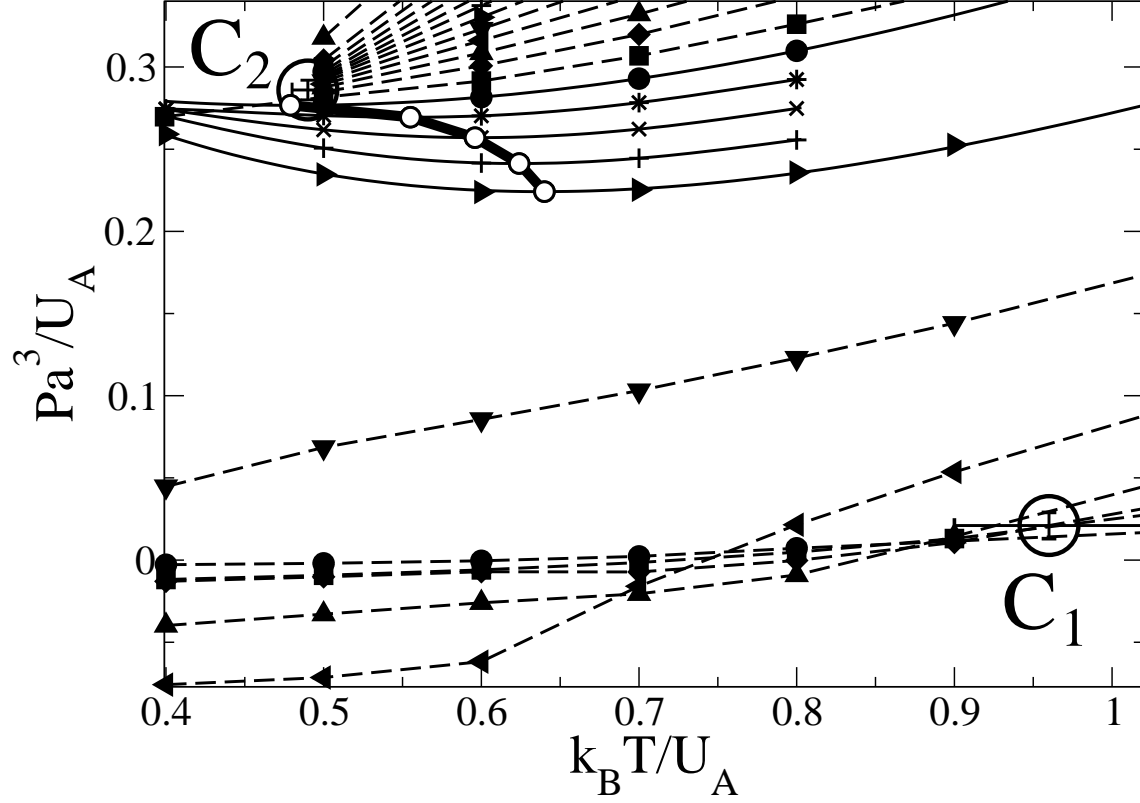


FIG. 5: The P - T phase diagram shows isochores with a clear minimum. The gas-liquid critical point C_1 and the liquid-liquid critical point C_2 are shown on the basis of the estimates in Figure 4. They are consistent with the crossing occurring at the highest T along each isochore. Symbols correspond to isochores for, from bottom to top at $k_B T/U_A = 1$, $\rho a^3 = 0.005, 0.075, 0.100, 0.125, 0.150, 0.175, 0.200, 0.205, 0.210, 0.215, 0.220, 0.225, 0.230, 0.235, 0.240, 0.245, 0.250, 0.255, 0.260, 0.265, 0.280, 0.290, 0.300, 0.310$. Dashed lines are a guide for the eyes. Solid lines are a quartic polynomial fit between the isochores showing a minimum. The open circles represent the point where $(\partial P/\partial T)_\rho = 0$ for the non-monotonic isochores. The thick gray line is a guide for the eyes representing an estimate of the T_{MD} temperature of maximum density at constant P . When not shown, errors are smaller than symbols size.

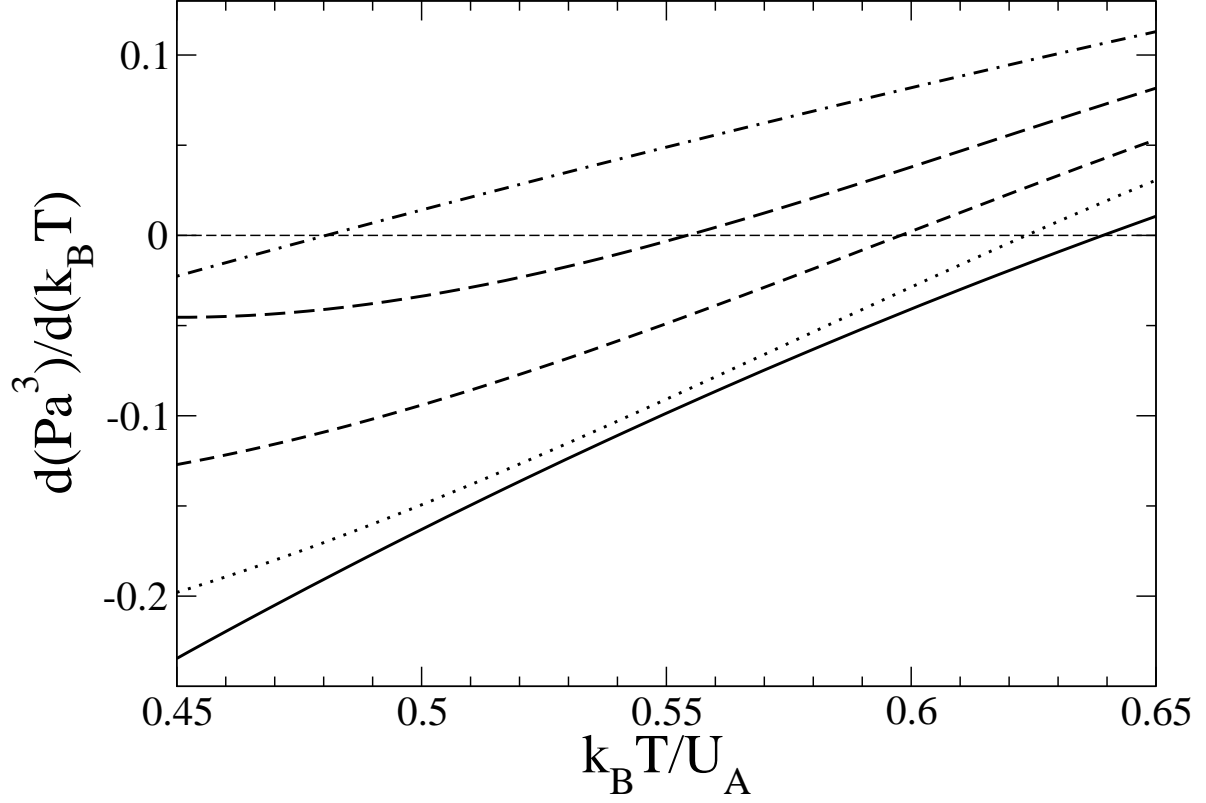


FIG. 6: Derivative of pressure with respect to temperature along the isochores at (from bottom to top) $\rho = 0.200, 0.205, 0.210, 0.215, 0.220$. Lines are plots of the cubic functions resulting from the derivative of the best-fit polynomials in Figure 5, with a relative errors on the parameters smaller than 10^{-3} . The temperature T^* where the derivative is zero is the minimum along the isochore, with $T^* = T_{\text{MD}}$ at the pressure corresponding to the state point at the given density and T^* .

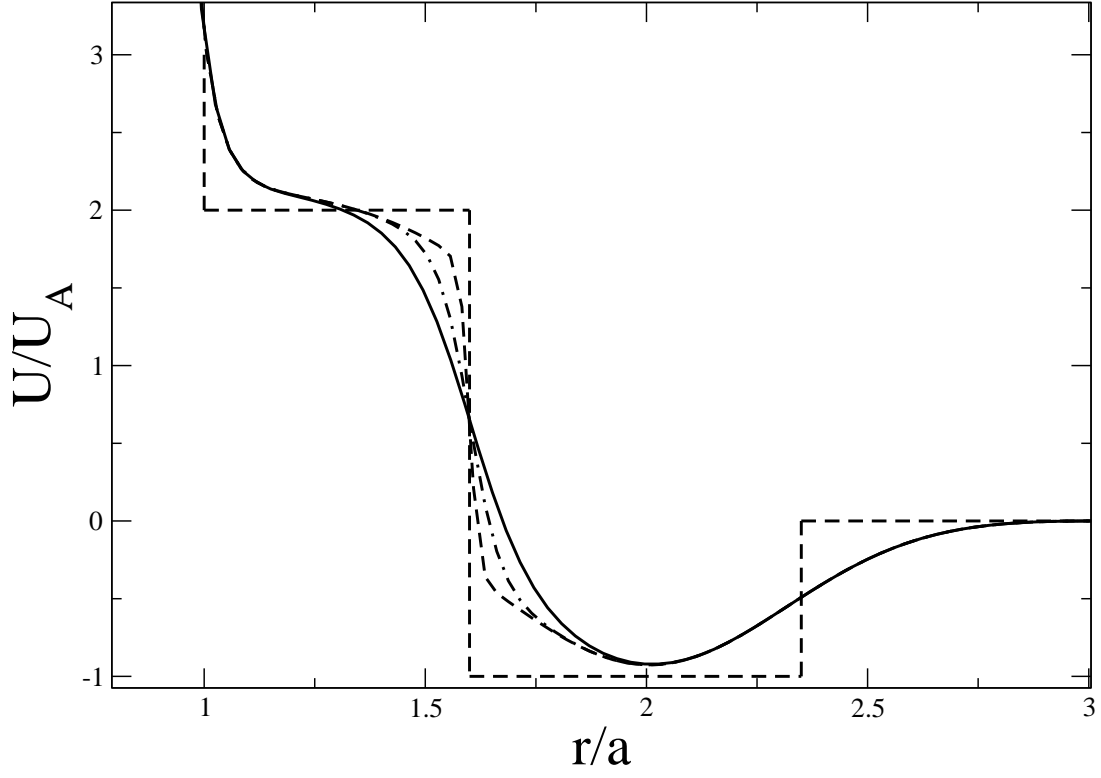


FIG. 7: The continuous potential can approximate the discontinuity at the repulsive distance $R_R/a = 1.6$ of the squared potential (thin dashed line) for increasing values of the parameter Δ , determining the slope at R_R . Continuous line is for $\Delta = 15$, studied in this work. Dash-dotted line is for $\Delta = 30$. Thick dashed line is for $\Delta = 100$.